Dalton Transactions

PAPER

View Article Online
View Journal | View Issue

Cite this: *Dalton Trans.*, 2014, **43**, 4720

Thermoelectric properties and electronic structure of the Zintl phase $Sr_5Al_2Sb_6$

Alex Zevalkink,†[a] Yoshiki Takagiwa,†[b] Koichi Kitahara,[b] Kaoru Kimura[b] and G. Jeffrey Snyder*[a]

Received 11th December 2013,
Accepted 7th January 2014

DOI: 10.1039/c3dt53487a

www.rsc.org/dalton

The Zintl phase $Sr_5Al_2Sb_6$ has a large, complex unit cell and is composed of relatively earth-abundant and non-toxic elements, making it an attractive candidate for thermoelectric applications. The structure of $Sr_5Al_2Sb_6$ is characterized by infinite oscillating chains of $AlSb_4$ tetrahedra. It is distinct from the structure type of the previously studied $Ca_5M_2Sb_6$ compounds (M = Al, Ga or In), all of which have been shown to have promising thermoelectric performance. The lattice thermal conductivity of $Sr_5Al_2Sb_6$ (~0.55 W mK^{-1} at 1000 K) was found to be lower than that of the related $Ca_5M_2Sb_6$ compounds due to its larger unit cell (54 atoms per primitive cell). Density functional theory predicts a relatively large band gap in $Sr_5Al_2Sb_6$, in agreement with the experimentally determined band gap of $E_g \sim 0.5$ eV. High temperature electronic transport measurements reveal high resistivity and high Seebeck coefficients in $Sr_5Al_2Sb_6$, consistent with the large band gap and valence-precise structure. Doping with Zn^{2+} on the Al^{3+} site was attempted, but did not lead to the expected increase in carrier concentration. The low lattice thermal conductivity and large band gap in $Sr_5Al_2Sb_6$ suggest that, if the carrier concentration can be increased, thermoelectric performance comparable to that of $Ca_5Al_2Sb_6$ could be achieved in this system.

Introduction

The thermal to electrical conversion efficiency of thermoelectric materials depends on the thermoelectric figure of merit, given by $zT = \frac{\sigma\alpha^2 T}{\kappa}$. An ideal thermoelectric material must strike a balance between the conflicting requirements of a high Seebeck coefficient, α, high electronic conductivity, σ, and low thermal conductivity, κ.[1] Zintl phases, with structures characterized by complex polyanions surrounded by highly electropositive cations, meet many of the criteria for successful thermoelectric materials.[2,3] In particular, they benefit from extremely low lattice thermal conductivity resulting from their complex unit cells,[4] and their electronic properties can often be finely tuned using chemical substitutions. Excellent thermoelectric performance ($zT > 1$) has been demonstrated in several Zintl phases,[5] including $Yb_{14}MnSb_{11}$ and $YbZn_{2-x}Cd_xSb_2$.[6,7] Many more Zintl phases, though not yet optimized for thermoelectric applications, appear to be promising candidates.[8–14]

Recently, we have shown that promising zT values can be achieved in compounds with chemical formulas $A_5M_2Sb_6$ and A_3MSb_3 (A = Ca, Sr and M = Al, Ga, In), which share a common structural motif: infinite chain-like polyanions formed from linked MSb_4 tetrahedra. These compounds have both low lattice thermal conductivity and sufficiently large band gaps for high temperature applications. By doping with Zn^{2+} on the M^{3+} site or Na^{1+} on the A^{2+} site, the charge carrier concentration of these compounds can be optimized, leading to figures of merit as high as $zT = 0.9$.[15–18]

Among $A_5M_2Sb_6$ compounds, most form either the $Ca_5Al_2As_6$ or $Ca_5Al_2Bi_6$ structure type.[19,20] These structure types both contain infinite chains of corner-linked MSb_4 tetrahedra in which neighboring chains are linked by Sb–Sb bonds to form ladder-like anionic structures. These two structure types differ only in the packing arrangement of the "ladders". $Sr_5Al_2Sb_6$ is the only exception, forming instead a completely unique structure type containing non-linear, oscillating chains, as shown in Fig. 1. The chains, which extend infinitely along the a-axis, are formed from alternately corner- and edge-sharing $AlSb_4$ tetrahedra, and oscillate back and forth along the c-axis. A repeat distance of four tetrahedra leads to a larger unit cell (4 formula units, or 52 atoms, per cell) than found in the other two $A_5M_2Sb_6$ structure types. In the original report of the $Sr_5Al_2Sb_6$ structure type,[21] Cordier *et al.* argue that this unique structure results from a combination of the relatively large cation (Sr) and small triel element (Al) in this compound.

Electron counting in $Sr_5Al_2Sb_6$ can be understood within the Zintl–Klemm formalism as follows: the two Sb that are

[a]*Materials Science, California Institute of Technology, 1200 E. California Blvd., Pasadena, CA 91125, USA. E-mail: jsnyder@caltech.edu*
[b]*Materials Science, The University of Tokyo, Japan*
†These authors contributed equally to this manuscript.

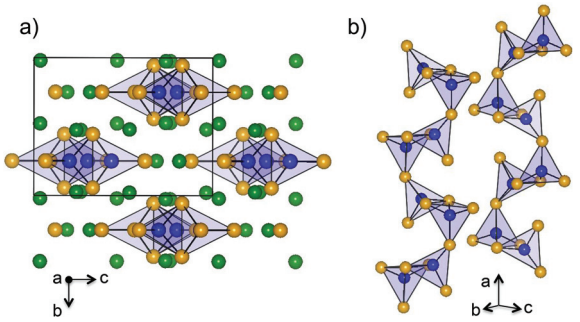

Fig. 1 (a) The orthorhombic structure of $Sr_5Al_2Sb_6$ (*Pnma*) is characterized by infinite anionic chains aligned in the [100] direction.[21] (b) Each chain is formed from alternately corner- and edge-sharing $AlSb_4$ tetrahedra. Sr atoms are shown in green, Sb in orange, and Al in blue.

singly-bonded to Al have a formal valence of 2−, while the corner-sharing and edge-sharing Sb (four per formula unit) each have a valence of 1−. The tetrahedrally coordinated Al atoms have a formal valence of 1−. Thus, in the covalent limit, the anionic unit can be written as $[(Al^{1-})_2(Sb^{2-})_2(Sb^{1-})_4]$, while the five Sr^{2+} atoms provide overall charge balance. Alternatively, if the Al atoms are treated as cations, the anionic unit can be written as $[(Al^{3+})_2(Sb^{4-})_2(Sb^{2-})_4]$.

From an application perspective, $Sr_5Al_2Sb_6$ is expected to have a lower lattice thermal conductivity than $Ca_5Al_2Sb_6$ due to its larger unit cell. Additionally, considering the expected electronic similarity of the two phases, one might expect subtle electronic effects to result from replacing Ca with Sr, despite their different structure types. For example, in AZn_2Sb_2 semiconducting compounds, the *A* species controls the hole concentration of the pure compound by influencing the equilibrium defect concentration.[33] The current study employs a combination of high temperature transport measurements and density functional theory to investigate the intrinsic thermoelectric properties of $Sr_5Al_2Sb_6$ and the effect of substituting Zn^{2+} on the Al^{3+} site.

Experimental

Computation

Density Functional calculations were performed with the WIEN2K code[22] based on the full-potential linearized augmented plane-wave (FP-LAPW) method under the generalized gradient approximation (GGA) as parameterized by Perdew, Burke, and Ernzerhof (PBE).[23] A plane wave basis cutoff of $R_{mt}K_{max}$ = 7 was used, in terms of the smallest muffin tin radius and maximum plane wave vector respectively. Muffin tin radii were 2.5 a.u. for Sr and 2.49 a.u. for both Al and Sb. Calculations were performed at the experimental lattice parameters (a = 12.124 Å, b = 10.341 Å, and c = 13.409 Å[21]). Self consistent calculations were performed with a 7 × 8 × 6 *k*-point mesh, and a 9 × 11 × 8 *k*-point mesh was used for calculating the Seebeck coefficients.

Synthesis

Bulk samples with nominal compositions of $Sr_5Al_2Sb_6$ and $Sr_5Al_{1.95}Zn_{0.05}Sb_6$ were prepared *via* ball milling followed by hot pressing, starting with elemental precursors. The elements (99% Sr pieces, 99% Al shot, 99.99% Zn shot, and 99.9999% Sb shot from Alfa Aesar) were cut into small pieces and loaded into stainless-steel vials, with stainless-steel balls in an Ar dry box. The contents were dry ball-milled for 1 h using a SPEX Sample Prep 8000 Series Mixer/Mill. The resulting fine powder was consolidated using a custom rapid hot press system[24] in high-density graphite dies (POCO) in argon for 3 h at 1073 K using 45 MPa of pressure, followed by a 3 h stress-free cool down.

Characterization

The hot-pressed, polycrystalline samples were sliced into 1 mm thick, 12 mm diameter disks. X-Ray diffraction was performed on polished slices using a Philips XPERT MPD diffractometer operated at 45 kV and 40 mA, and Rietveld analysis was performed using Rigaku PDXL software. High temperature electronic properties were characterized up to 973 K under dynamic vacuum. Electrical resistivity was measured using the Van der Pauw technique and the Hall coefficient was measured with a 2 T field and pressure-assisted tungsten contacts.[25] The Seebeck coefficients were measured using chromel-Nb thermocouples by allowing the temperature gradient across the sample to oscillate between ±10 K, as described in ref. 26. A Netzch LFA 457 was used to measure the thermal diffusivity.

Results and discussion

Electronic structure

Density functional theory (DFT) calculations confirm that $Sr_5Al_2Sb_6$ has a fully filled valence band and an empty conduction band, as expected for a classic Zintl phase. The predicted band gap is approximately 0.8 eV. As illustrated by the electronic density of states in Fig. 2, the valence band maximum and the conduction band minimum are composed primarily of Sb and Al electronic states, resulting, respectively, from Al–Sb bonding and anti-bonding interactions. Strong Sr character is most apparent deep in the conduction band. Similar characteristics of the electronic structure were also observed in the related $A_5M_2Sb_6$ and A_3MSb_3 Zintl phases (A = Ca, Sr and M = Al, Ga, In).[15,16,27] Semi-classical Boltzmann transport theory was employed to calculate the Seebeck coefficient, α, as a function of temperature in the three principle directions, as shown in the inset of Fig. 2. The resulting values are consistent with the experimental results (unfilled symbols) for the undoped $Sr_5Al_2Sb_6$ discussed below.

Electronic transport

The $Sr_5Al_2Sb_6$ samples synthesized by ball milling followed by hot pressing were dense and at least 95% phase pure. A representative X-ray diffraction pattern and Rietveld fit for an

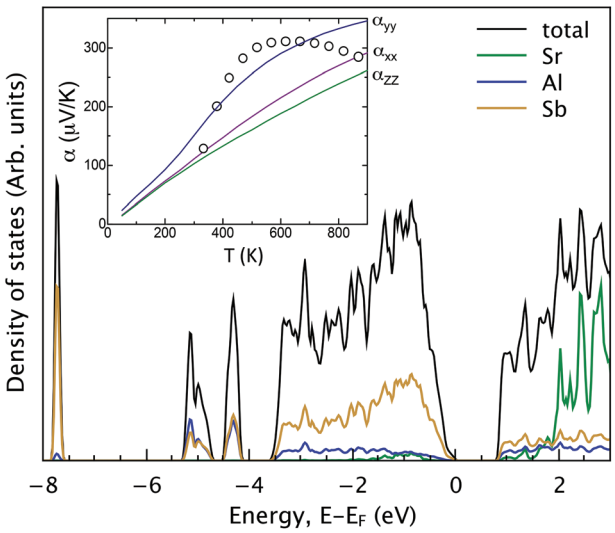

Fig. 2 The electronic density of states of $Sr_5Al_2Sb_6$ shows a fully filled valence band and a relatively large band gap of 0.8 eV. The inset shows the calculated and experimental Seebeck coefficients as a function of temperature.

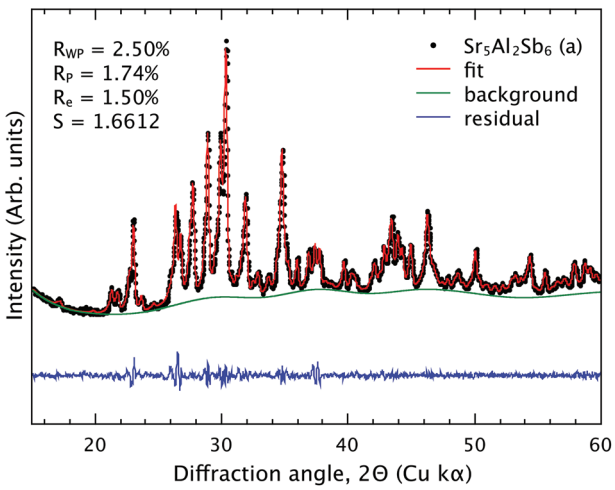

Fig. 3 Rietveld analysis of the X-ray diffraction data for hot-pressed $Sr_5Al_2Sb_6$ suggests that the samples are phase pure.

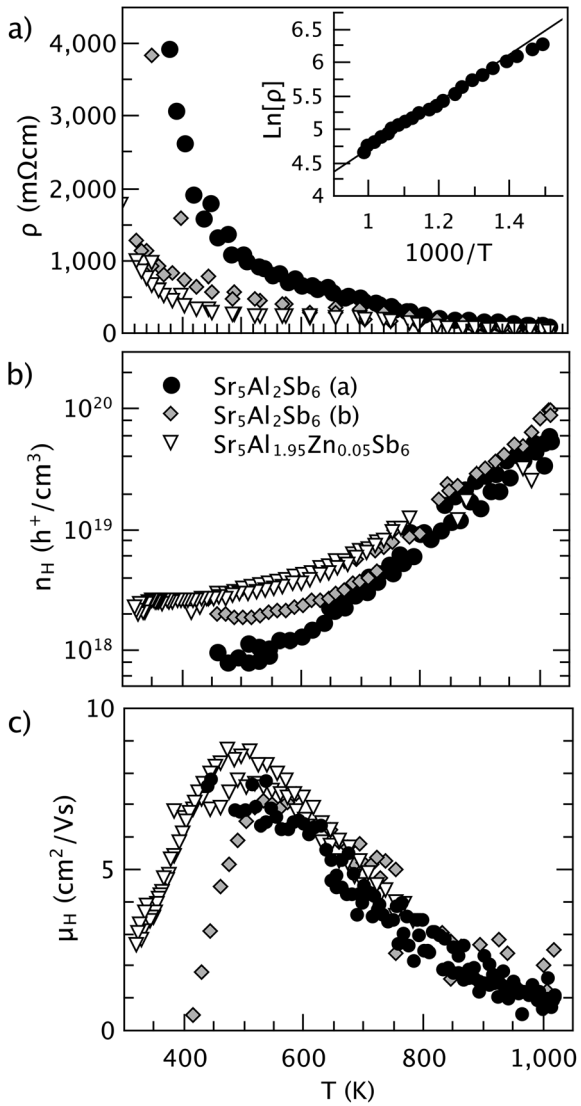

Fig. 4 (a) $Sr_5Al_2Sb_6$ samples behave as intrinsic semiconductors with resistivity that decreases with temperature and (b) carrier concentration that increases with temperature. (c) The magnitude of the mobility is comparable to $Ca_5M_2Sb_6$ phases.

undoped sample is shown in Fig. 3, and shows no sign of significant impurity phases.

Fig. 4a–c shows the resistivity (ρ), Hall carrier concentration (n_H) and mobility (μ_H) for two different undoped $Sr_5Al_2Sb_6$ samples and one Zn-containing sample with a synthetic composition of $Sr_5Al_{1.95}Zn_{0.05}Sb_6$. Consistent with the calculated electronic structure, undoped $Sr_5Al_2Sb_6$ samples are found to behave as intrinsic semiconductors. The resistivity, shown in Fig. 4a, is very high at room temperature and decreases exponentially with increasing temperature. Using the relation $\rho \propto e^{E_g/2kT}$ for intrinsic semiconductors, a band gap of $E_g \sim 0.5$ eV was obtained from the resistivity of sample (a) at high temperature.

The undoped samples have positive carrier concentrations, indicating that $Sr_5Al_2Sb_6$ is naturally slightly p-type, most likely due to small deviations from the nominal stoichiometry. At room temperature, n_H is quite low (~10^{18} holes per cm^3), and increases with increasing temperature due to the thermal activation of carriers across the band gap. In Zintl compounds with the chemical formula AZn_2Sb_2 (A = Sr, Ca, Eu, Yb), the cation was found to play an important role in determining the stable concentration of A vacancies, thus determining the p-type carrier concentration at room temperature.[33] $SrZn_2Sb_2$ was found to have the lowest hole concentration among compounds in that system. Among $A_5Al_2Sb_6$ compounds, we find that the Sr analogue also has fewer holes (<2 × 10^{18} holes per cm^3) than the Ca-based compounds (>5 × 10^{18} holes per cm^3), perhaps due to a similar mechanism.

The nominally Zn-doped sample ($Sr_5Al_{1.95}Zn_{0.05}Sb_6$) is expected to have a carrier concentration of approximately 1.2×10^{20} h^+ cm^{-3}, assuming that each Zn substitution leads to one free carrier. Experimentally, however, the measured carrier concentration of the Zn-doped sample is only slightly higher than that of the undoped samples, suggesting that Zn may have very limited solubility in the $Sr_5Al_2Sb_6$ structure. This is in contrast to $Ca_5Al_2Sb_6$, in which the substitution of Zn^{2+} on the Al^{3+} site leads to an increase in carrier concentration by two orders of magnitude and a clear transition from non-degenerate to degenerate semiconducting behavior.[28] Structural differences between the $A_5Al_2Sb_6$ phases, in addition to the possible influence of the cation on the stability of acceptor defects (*e.g.*, Sr vacancies and Zn substitution on Al site), could explain this disparity. In previous studies, Na^{1+} on the Ca^{2+} site was a successful dopant in both $Ca_5Al_2Sb_6$ and Ca_3AlSb_3 compounds,[16,18] suggesting that similar substitutions may prove successful in increasing the carrier concentration in $Sr_5Al_2Sb_6$.

The Hall mobility of both undoped and Zn-doped samples increases with increasing temperature below 500 K, suggesting an activated process ($\mu_H \propto e^{E_A/k_BT}$) arising from an oxide layer or secondary phase at the grain boundaries. At temperatures above 500 K the mobility is limited by acoustic phonon scattering, for which the temperature dependence is given by $\mu_H \propto T^{-\nu}$, where ν ranges from 1 to 1.5 for degenerate and non-degenerate behavior, respectively.[29] The magnitude of the mobility (8 cm^2 V^{-1} s^{-1} at 300 K) is comparable to that of $Ca_5Al_2Sb_6$ and $Ca_5In_2Sb_6$.[27]

Shown in Fig. 5, the Seebeck coefficients of the undoped sample (a) are large and positive, consistent with the low p-type carrier concentration and high resistivity. Above 600 K, the Seebeck coefficients begin to decrease due to minority carrier effects. Estimating the band gap from the peak Seebeck coefficient ($E_g = 2\alpha_{max}T_{max}$) yields E_g = 0.4 eV, comparable to the value obtained from the resistivity.

The effective mass of the valence band in $Sr_5Al_2Sb_6$ can be estimated from the experimental Seebeck coefficients and carrier concentrations using a single parabolic band model (SPB). Because this model assumes that only a single carrier type is present, the model must be employed at temperatures below the onset of minority carrier activation (approximately 500 K, in this case). At 500 K, an SPB model yields an effective valence band mass of approximately 0.3 m_e. This is dramatically lower than that of $Ca_5M_2Sb_6$ ($m^*_{SPB} \sim 2\ m_e$) compounds, which is surprising, given that the electronic mobilities in those compounds are quite similar. This inconsistency may arise from several explanations, including a reduced carrier relaxation time (τ) in $Sr_5Al_2Sb_6$ from mechanisms other than reduced m^* (*e.g.* increased deformation potential[30]), or non-degenerate behavior in the undoped sample even below 500 K leading to a compensated Seebeck coefficient.

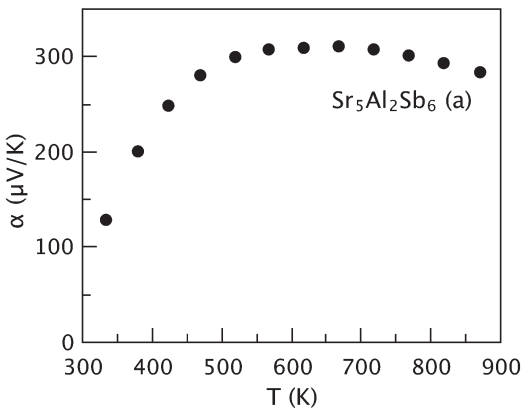

Fig. 5 The high, positive Seebeck coefficient is consistent with the low, p-type carrier concentration and intrinsic behavior.

Thermal transport

The primary attraction of Zintl compounds for thermoelectric applications is their extremely low lattice thermal conductivity (κ_L), which arises from their complex crystal structures.[4] In $Sr_5Al_2Sb_6$, a single unit cell contains 52 atoms, meaning that much of the heat capacity is trapped in flat, low velocity optical modes, thus suppressing κ_L. The thermal conductivity of $Sr_5Al_2Sb_6$, shown in Fig. 6, is calculated from the thermal diffusivity, D, using $\kappa = DC_Pd$. Here, C_P is the Dulong–Petit heat capacity (0.27 J g^{-1} K^{-1}) and d is the geometric density (4.27 g cm^{-3}). The electronic contribution to κ is negligible due to the high electrical resistivity, and κ can thus be considered equivalent to the lattice thermal conductivity. The minimum lattice thermal conductivity (dashed line in Fig. 6) of $Sr_5Al_2Sb_6$ was calculated using relationship giving by Cahill *et al.* in ref. 31 with the measured longitudinal and transverse speeds of sound of 3720 m s^{-1} and 2050 m s^{-1}, respectively.

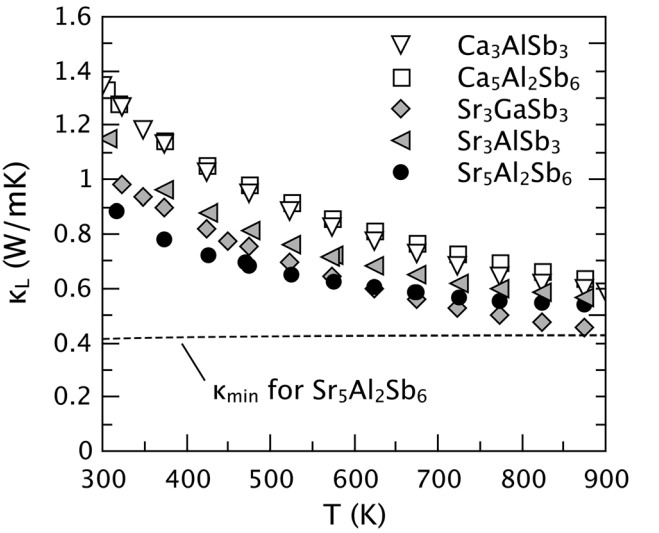

Fig. 6 The lattice thermal conductivity of $Sr_5Al_2Sb_6$ compared with other chain-forming $A_5M_2Sb_6$ and A_3MSb_3 compounds (A = Ca, Sr and M = Al, Ga, In).[15–18] Compounds with 52 or 56 atoms per unit cell are denoted by grey or black filled symbols, while those with 26 or 28 atoms are denoted by unfilled symbols.

We have previously reported exceptionally low κ_L in several other chain-forming $A_5M_2Sb_6$ and A_3MSb_3 compounds (A = Ca, Sr and M = Al, Ga, In).[15–18] The temperature dependence of κ_L in $Sr_5Al_2Sb_6$ is very similar to these compounds, decreasing as $1/T$ with increasing temperature due to Umklapp scattering, and approaching the predicted minimum at high temperature. Because the unit cell size and average speed of sound of $Sr_5Al_2Sb_6$ (52 atoms, 2610 m s^{-1}) are comparable to that of Sr_3AlSb_3 (56 atoms, 2590 m s^{-1}), κ_L should be very similar in these two materials, despite their different structure types.[4] Indeed, at high temperature, κ_L is nearly identical in $Sr_5Al_2Sb_6$ and Sr_3AlSb_3, reaching values of 0.54 W mK^{-1} and 0.60 W mK^{-1}, respectively. However, at 300 K, κ_L of $Sr_5Al_2Sb_6$ is significantly lower than Sr_3AlSb_3, suggesting that an additional scattering mechanism such as boundary or point defect scattering is also present.

Figure of merit

The thermoelectric figure of merit of undoped $Sr_5Al_2Sb_6$ is only 0.05 at 800 K, due to the low carrier concentration and intrinsic electronic properties of this material. This low value is comparable to the low zT found in undoped, intrinsic $Ca_5M_2Sb_6$ compounds (M = Al, Ga, or In), which, upon doping, exhibit zT values up to 0.7. In both $Ca_5Al_2Sb_6$ and $Ca_5In_2Sb_6$ the zT is optimized at carrier concentrations near 2×10^{20} h^+ cm^{-3}, or two orders of magnitude higher than the samples in this study. Unfortunately, in the present study, doping with Zn failed to appreciably increase the carrier concentration. However, different dopants (*e.g.*, Na^{1+} or K^{1+} on the Sr^{2+} site) may prove successful in future studies, and thus lead to a significant increase in both the carrier concentration and peak zT in this material. For example, in the Zintl phase Ca_3AlSb_3, doping with Na on the Ca site was found to be more effective at increasing the p-type carrier concentration than substitution Zn on the Al site.[16,32]

Conclusion

$Sr_5Al_2Sb_6$ is a valence-precise Zintl phase exhibiting thermal and electronic properties comparable to the intrinsic properties of previously investigated $Ca_5M_2Sb_6$ compounds. Density functional theory (DFT) shows that $Sr_5Al_2Sb_6$ has a fully filled valence band dominated by Sb and Al electronic states and a sufficiently large band gap for thermoelectric applications. Electronic transport measurements reveal intrinsic semiconducting behavior and a very low p-type carrier concentration. The magnitude of the electronic mobility of $Sr_5Al_2Sb_6$ is comparable to that of undoped $Ca_5Al_2Sb_6$, although the band mass, estimated from the experimental Seebeck coefficient, is considerably smaller. Due to its large, complex unit cell and low speed of sound, $Sr_5Al_2Sb_6$ has exceptionally low lattice thermal conductivity. Although doping with Zn did not increase the carrier concentration in this study, the intrinsic thermal and electronic properties of $Sr_5Al_2Sb_6$ suggest that significantly higher zT values can potentially be obtained in optimally doped $Sr_5Al_2Sb_6$.

Acknowledgements

We gratefully acknowledge the Jet Propulsion Laboratory for support. Yoshiki Takagiwa acknowledges support from the Sumitomo Foundation (grant no. 120567) and the Murata Science Foundation.

References

1 G. J. Snyder and E. S. Toberer, Complex thermoelectric materials, *Nat. Mater.*, 2008, **7**, 105–114.
2 S. M. Kauzlarich, *Chemistry, Structure, and Bonding of Zintl Phases and Ions*, Wiley-VCH, 1996.
3 M. Mills, R. Lam, M. J. Ferguson, L. Deakin and A. Mar, Chains, planes, and antimonides, *Coord. Chem. Rev.*, 2002, **233–234**, 207–222.
4 E. S. Toberer, A. Zevalkink and G. J. Snyder, Phonon engineering through crystal chemistry, *J. Mater. Chem.*, 2011, **21**(40), 15843.
5 E. S. Toberer, A. F. May and G. J. Snyder, Zintl Chemistry for Designing High Efficiency Thermoelectric Materials, *Chem. Mater.*, 2010, **22**(3), 624–634.
6 K. Guo, Q.-G. Cao, X.-J. Feng, M.-B. Tang, H.-H. Chen, X. Guo, L. Chen, Y. Grin and J.-T. Zhao, Enhanced thermoelectric figure of merit of Zintl phase $YbCd_{2-x}Mn_xSb_2$ by chemical substitution, *Eur. J. Inorg. Chem.*, 2011, **2011**(26), 4043–4048.
7 E. S. Toberer, C. A. Cox, S. R. Brown, T. Ikeda, A. F. May, S. M. Kauzlarich and G. J. Snyder, Traversing the metal-insulator transition in a Zintl phase: rational enhancement of thermoelectric efficiency in $Yb_{14}Mn_{1-x}Al_xSb_{11}$, *Adv. Funct. Mater.*, 2008, **18**(18), 2795–2800.
8 A. P. Holm, S.-M. Park, C. L. Condron, H. Kim, P. Klavins, F. Grandjean, R. P. Hermann, G.-J. Long, M. G. Kanatzidis and S. M. Kauzlarich, $Eu_{10}Mn_6Sb_{13}$: A new ternary rare-earth transition metal Zintl phase, *Inorg. Chem.*, 2003, **42**, 4660–4667.
9 J. Wang, S. Q. Xia and X. T. Tao, $A_{10}LaCdSb_9$ (A = Ca,Yb): a highly complex Zintl system and the thermoelectric properties, *Chem.–Asian J.*, 2013, **8**, 251–257.
10 J. Wang, M. Yang, M. Y. Pan, S. Q. Xia, X. T. Tao, H. He, G. Darone and S. Bobev, Synthesis, crystal and electronic structures, and properties of the new pnictide semiconductors A_2CdPn_2 (A = Ca, Sr, Ba, Eu; Pn = P, As), *Inorg. Chem.*, 2011, **50**, 8020–8027.
11 S.-M. Park, S.-J. Kim and M. G. Kanatzidis, A unique framework in $BaGa_2Sb_2$: a new Zintl phase with large tunnels, *Inorg. Chem.*, 2001, **40**, 3781–3785.
12 S.-J. Kim, S. Hu, C. Uher and M. G. Kanatzidis, $Ba_4In_8Sb_{16}$: Thermoelectric Properties of a New Layered Zintl Phase

with Infinite Zigzag Sb Chains and Pentagonal Tubes, *Chem. Mater.*, 1999, **11**, 3154–3159.

13 S. M. Park, S.-J. Kim and M. G. Kanatzidis, $Eu_7Ga_6Sb_8$: A Zintl phase with Ga-Ga bonds and polymeric gallium antimonide chains, *J. Solid State Chem.*, 2004, **177**, 2867–2874.

14 R. Lam and A. Mar, Synthesis and Structure of $Ba_2Sn_3Sb_6$, a Zintl Phase Containing Channels and Chains, *Inorg. Chem.*, 1996, **35**, 6959–6963.

15 A. Zevalkink, W. G. Zeier, G. Pomrehn, E. Schechtel, W. Tremel and G. J. Snyder, Thermoelectric properties of Sr_3GaSb_3, a chain-forming Zintl compound, *Energy Environ. Sci.*, 2012, **5**(10), 9121.

16 A. Zevalkink, E. S. Toberer, W. G. Zeier, E. Flage-Larsen and G. J. Snyder, Ca_3AlSb_3: an inexpensive, non-toxic thermoelectric material for waste heat recovery, *Energy Environ. Sci.*, 2011, **4**(2), 510.

17 A. Zevalkink, J. Swallow and G. J. Snyder, Thermoelectric properties of Zn-doped $Ca_5In_2Sb_6$, *Dalton Trans.*, 2013, **42**, 9713–9719.

18 E. S. Toberer, A. Zevalkink and G. Snyder, The Zintl compound $Ca_5Al_2Sb_6$ for low cost thermoelectric power generation, *Adv. Funct. Mater.*, 2010, **20**, 4375–4380.

19 G. Cordier, E. Czech, M. Jakowski and H. Schaefer, Zintlphasen mit komplexen anionen: zur kenntnis von $Ca_5Al_2Sb_6$ und $Ca_3Al_2As_4$, *Rev. Chim. Miner.*, 1981, **18**, 9–18.

20 I. Todorov, D. Y. Chung, L. Ye, A. J. Freeman and M. G. Kanatzidis, Synthesis, structure and charge transport properties of $Yb_5Al_2Sb_6$: a Zintl phase with incomplete electron transfer, *Inorg. Chem.*, 2009, **48**(11), 4768–4776.

21 G. Cordier and M. Stelter, $Sr_5Al_2Sb_6$ und $Ba_5In_2Sb_6$: zwei neue Zintlphasen mit unterschiedlichen Baenderanionen, *Z. Naturforsch*, 1988, **43b**, 463–466.

22 P. Blaha, K. Schwarz, G. Madsen, D. Kvasnicka and J. Luitz, *WIEN2k: an augmented plane wave plus local orbitals program for calculating crystal properties*, Institute of Physical and Theoretical Chemistry, TU Vienna, 2001.

23 J. P. Perdew, K. Burke and M. Ernzerhof, Generalized gradient approximation made simple, *Phys. Rev. Lett.*, 1996, **77**, 3865–3868.

24 A. D. LaLonde, T. Ikeda and G. J. Snyder, Rapid consolidation of powdered materials by induction hot pressing, *Rev. Sci. Instrum.*, 2011, **82**, 025104.

25 K. A. Borup, E. S. Toberer, L. Zoltan, G. Nakatsukasa, M. Errico, J. Fleurial, B. Iverson and G. J. Snyder, Measurement of the Electrical Resistivity and Hall Coefficient at High Temperatures, *Rev. Sci. Instrum.*, 2012, **83**, 123902.

26 S. Iwanaga, E. S. Toberer, A. LaLonde and G. J. Snyder, A high temperature apparatus for measurement of the Seebeck coefficient, *Rev. Sci. Instrum.*, 2011, **82**(6), 063905.

27 A. Zevalkink, G. S. Pomrehn, S. Johnson, J. Swallow, Z. M. Gibbs and G. J. Snyder, Influence of the triel elements (M = Al, Ga, In) on the transport properties of $Ca_5M_2Sb_6$ Zintl compounds, *Chem. Mater.*, 2012, **24**(11), 2091–2098.

28 A. Zevalkink, E. S. Toberer, T. Bleith, E. Flage-Larsen and G. J. Snyder, Improved carrier concentration control in Zn-doped $Ca_5Al_2Sb_6$, *J. Appl. Phys.*, 2011, **110**(1), 013721.

29 U. I. Ravich, B. A. Efimova and I. A. Smirnov, *Semiconducting lead chalcogenides*, Plenum Press, 1970.

30 H. Wang, Y. Z. Pei, A. D. LaLonde and G. J. Snyder, Weak electron phonon coupling contributing to high thermoelectric performance in n-type PbTe, *Proc. Natl. Acad. Sci. U. S. A.*, 2011, **109**, 9705–9709.

31 D. Cahill, S. Watson and R. Pohl, Lower limit to the thermal conductivity of disordered crystals, *Phys. Rev. B: Condens. Matter*, 1992, **46**(10), 6131–6140.

32 W. G. Zeier, A. Zevalkink, E. Schechtel, W. Tremel and G. J. Snyder, Thermoelectric properties of Zn-doped Ca_3AlSb_3, *J. Mater. Chem.*, 2012, **22**(19), 9826.

33 G. Pomrehn, A. Zevalkink, W. Zeier, A. Van der Walle and G. J. Snyder, Defect-controlled electronic properties in AZn_2Sb_2 Zintl phases (A = Ca, Sr, Eu, Yb), *Angew. Chem.*, 2014, accepted.